

Cyano-Based Materials with Giant Optical Anisotropy and Second Harmonic-Generation Effect

Lei Kang,^{†,‡,§} Fei Liang,^{§,⊥} Zheshuai Lin,^{*,§} Feng Liu,^{‡,§} and Bing Huang^{*,†}

[†]Beijing Computational Science Research Center, Beijing 100193, China

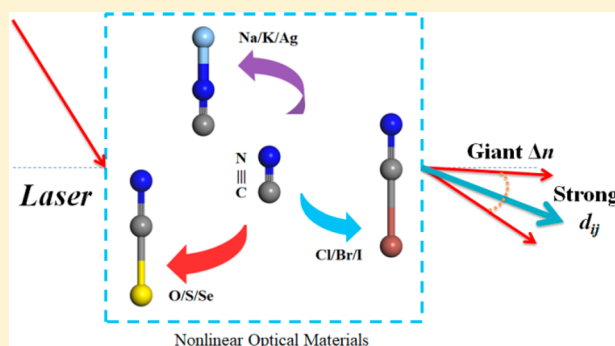
[§]Technical Institute of Physics and Chemistry, Chinese Academy of Sciences, Beijing 100190, China

[‡]Department of Materials Science and Engineering, University of Utah, Salt Lake City, Utah 84112, United States

[⊥]University of Chinese Academy of Sciences, Beijing 100190, China

Supporting Information

ABSTRACT: It is a huge challenge to achieve giant optical anisotropy (e.g., birefringence) over a wide region from infrared (IR) to ultraviolet (UV) spectroscopy. This is mainly due to the lack of ideal optical motifs, which should have giant structural anisotropy with a wide transparent range. Especially in the field of nonlinear optical (NLO) materials, polar motifs with giant optical anisotropy are extremely scarce, but they are favorable to exhibit strong second harmonic generation (SHG) effect and phase-matching capacity. On the basis of analysis of microstructure and macro optical property, in this study, we focus on one-dimensional chained cyano (CN) motif and surprisingly find that it can exhibit sufficiently large optical anisotropy and SHG effect from IR to UV regions. Therefore, it is reasonable to believe that the CN motif can be considered as a novel NLO material gene, which was totally ignored in the previous studies. Interestingly, the CN-gene can be integrated into various coordination structures, such as metal cyanides, cyanogen halides, and cyanogen chalcogenides, to promote these materials to exhibit tunable NLO capabilities from IR to UV and deep-UV regions. Remarkably, the chained acentric CNI structure, which has already been obtained in the experiment, can achieve the IR and UV frequency conversion with a sufficiently large SHG effect (~ 17 pm/V) and a giant optical birefringence (~ 0.7 at 1064 nm). Therefore, the cyano-based compounds proposed in this article can not only enrich the structural chemistry of NLO materials, but also potentially advance the development of optical material genome project.



1. INTRODUCTION

Optical anisotropy is very important for linear and nonlinear optical (NLO) components,¹ which can greatly enhance the NLO response and phase-matching capacity of a NLO material for tunable frequency conversion.^{2,3} For decades, the development of NLO crystals has progressed at a rapid rate, so that tunable coherent radiation with high-output power can be easily obtained from ultraviolet (UV) to infrared (IR) spectral regions of 0.2–2 μm . However, it is still a big challenge to achieve giant optical anisotropy and second harmonic generation (SHG) effect in the regions from UV to IR. This is mainly due to the lack of ideal NLO motifs, which should have giant structural anisotropy with a wide transparency beyond conventional NLO structural motifs such as $(\text{BO}_3)^{3-}$ in $\text{KBe}_2\text{BO}_3\text{F}_2$ (KBBF),⁴ $(\text{B}_3\text{O}_6)^{3-}$ in $\beta\text{-BaB}_2\text{O}_4$ (BBO),⁵ $(\text{B}_3\text{O}_7)^{5-}$ in LiB_3O_5 (LBO),⁶ $(\text{H}_2\text{PO}_4)^-$ in KH_2PO_4 (KDP),⁷ $(\text{TiO}_6)^{8-}$ in KTiOPO_4 (KTP),⁷ $(\text{NbO}_6)^{7-}$ in LiNbO_3 (LN),⁸ and $(\text{GaS}_4)^{5-}$ in AgGaS_2 (AGS).⁹

In general, an available NLO crystal must satisfy: (i) a strong NLO response, mainly corresponding to the SHG coefficients d_{ij} ; (ii) a large birefringence Δn that requires the dispersion of

the refractive indices n to satisfy the condition of $n_{\text{max}}(2\lambda_{\text{PM}}) = n_{\text{min}}(\lambda_{\text{PM}})$, where λ_{PM} is the shortest phase-matching wavelength; and (iii) a short UV absorption edge λ_{UV} that are determined by the energy bandgap E_g .^{10,11} Especially in the deep-UV region, sufficiently large birefringence (usually >0.07 at 1064 nm) is very necessary for the deep-UV SHG output. To date only a few deep-UV optical materials can satisfy the requirements.^{12,13} KBBF is now the only practically used deep-UV NLO material with $\lambda_{\text{UV}} = 148$ nm, $\Delta n = 0.077$, and $d_{22} = 1.2 \times \text{KDP}$ (d_{36} of KDP = 0.39 pm/V).⁴ Even in the IR region, large birefringence is still very important for frequency conversion when the most practical Nd:YAG 1064 nm laser is applied. However, sufficiently large birefringence is rare in the transparent range from IR to UV and deep-UV regions. As a typical birefringent crystal, BBO has a birefringence about 0.12 at 1064 nm. For a IR optical material, it can be enlarged to 0.30 although giant birefringence (e.g., >0.70) is still scarce.¹ In addition, large SHG effect is also needed to

Received: October 1, 2018

Published: November 13, 2018

guarantee a high conversion efficiency.^{14,15} Basically, SHG effect decreases with energy bandgap increases. Therefore, it is difficult to find a balance both with strong SHG effect and large bandgap. For example, for the typical IR NLO material LN, its SHG effect is about $10 \times$ KDP but bandgap is 3.0 eV.⁸ Although for the typical UV NLO material BBO, its bandgap is 6.9 eV although SHG effect is about $3 \times$ KDP.⁵ The reason is that the NLO active units, e.g., $(\text{NbO}_6)^{7-}$ in LN or $(\text{B}_3\text{O}_6)^{3-}$ in BBO, have insufficiently large optical anisotropy. Therefore, it is meaningful to search for an available NLO-balanced motif with wide bandgap E_g , strong SHG effect d_{ij} as well as large optical birefringence Δn .

With the development of density-functional theory (DFT) and Material Genome Initiative, high-performing theoretical simulations have become an effective and efficient method to search for new NLO materials that are possible to possess unexpected capabilities.^{15,16} Accordingly in this work, we find that one-dimensional (1D) chained cyano (CN) motif can be considered as a novel NLO material gene with large bandgap E_g , SHG effect d_{ij} and birefringence Δn . By engineering it into various coordination structures, the CN-gene can exhibit giant optical anisotropy and tunable NLO capability. Furthermore, the structure–property correlations of several CN-based material systems are studied systematically and their NLO performances are evaluated.

2. COMPUTATIONAL METHODS

The DFT calculations are performed using the plane-wave pseudopotential method implemented in the CASTEP package.^{17,18} Optimized norm-conserving pseudopotentials are adopted for all elements.¹⁹ A series of computational parameters with high-precision including a kinetic energy cutoff >700 eV, a self-consistent-field tolerance of 5.0×10^{-8} eV per atom and Monkhorst-Pack k -point meshes spanning less than 0.04 per \AA^3 in the Brillouin zone.²⁰ The unit cell parameters and atomic positions are further optimized using the quasi-Newton method.²¹ The convergence thresholds between optimization cycles for convergence of energy, force, stress, and displacement are set as 5.0×10^{-6} eV per atom, 0.01 eV per \AA , 0.02 GPa, and 5.0×10^{-4} \AA , respectively. On the basis of the optimized structures and ground-state calculations, the electronic band structures and optical properties can be obtained according to the proposed methods.¹⁶ Accordingly, the energy bandgap E_g is calculated from the screened exchange local density approximation (sX-LDA) functional,²² whereas the optical properties are calculated by the scissors-corrected LDA method,²³ where the scissors operator is set as the difference between the sX-LDA and LDA bandgaps. This self-consistent ab initio approach has proven to be an efficient way to study the NLO properties in many semiconductor materials without introducing any experimental parameter.¹⁶ As a result, the refractive indices n and the birefringence Δn are obtained.¹² Moreover, SHG coefficients d_{ij} are calculated using the expressions developed by Lin et al.²⁴

As a typical NLO material containing CN bond, urea with the chemical formula $\text{CO}(\text{NH}_2)_2$ (for crystal structure, see Figure S1) is selected as the reference benchmark for calculations.²⁵ Its unit cell parameters are optimized and optical properties are calculated to show the accuracy of our proposed method for CN-based systems. It is shown from Table 1 that the relative error of lattice constants and bond lengths between calculations and experiments is less than 5%. The calculated energy bandgap and birefringence (6.20 eV and 0.113) are in quite good agreement with the experimental values (6.18 eV and 0.102). Although the calculated SHG coefficient d_{36} (~ 1.87 pm/V) is larger than the experimental result (~ 1.30 pm/V), it can be still compared as the benchmark of SHG effect. The consistence with the experimental results demonstrates the validity of our computational methods for the present purposes.

Table 1. Structural Parameters, Bond Lengths, and NLO Properties of the Urea Crystal $\text{CO}(\text{NH}_2)_2$

	unit-cell parameters				bond length (\AA)		
	$a = b$ (\AA)	c (\AA)	$\alpha = \beta = \gamma$ (deg)	V (\AA^3)	C–N	C–O	N–H
expt	5.645	4.704	90	149.898	1.333	1.246	1.005
calc	5.333	4.462	90	126.918	1.340	1.192	1.032
	E_g (eV)	d_{ij} (pm/V)	$d_{36}^{\text{max}}/d_{36}(\text{KDP})^a$		Δn at 1064 nm	λ_{UV} (nm)	
expt	6.18	$d_{36} = 1.30$	3.33		0.102	200	
calc	6.20	$d_{36} = 1.87$	4.79		0.113	200	

^a d_{36} of KDP = 0.39 pm/V.

3. RESULTS AND DISCUSSION

The structure–property relationship of NLO materials have been well understood in the past 20 years.^{12,26} In addition, several theoretical and semiempirical methods were proposed in our previous studies, and have been verified by experiments.^{27–33} A NLO crystal should consist of some NLO-active units with large structural anisotropy such as 2D layers or 1D chains. Such a structural feature could not only keep an effective SHG effect, but also exhibit an efficient optical birefringence.³⁴ If the nonbonding states around the band edges are removed as much as possible, the bandgap can be enlarged.²⁷ BBO and HgBr_2 are two typical structures with 2D $(\text{B}_3\text{O}_6)^{3-}$ planes and 1D Br–Hg–Br chains, respectively.^{5,35}

In this study, cyano (CN) group, which consists of a carbon atom triple-bonded to a nitrogen atom, is such a NLO-active gene with favorable 1D dipole structure and coordination diversity (see Figure 1). Depending on this CN unit, the urea

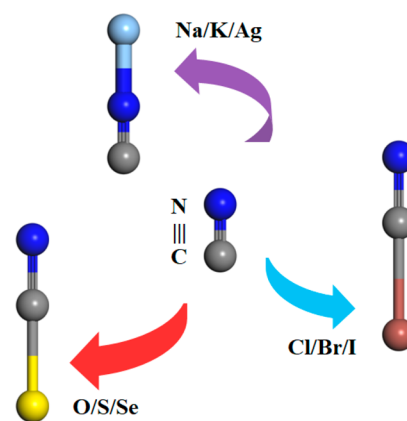


Figure 1. Molecular structural diversity of cyano group.

crystal is an important UV NLO material with large Δn (~ 0.1).²⁵ For urea, however, its λ_{UV} (~ 200 nm) is not deep-UV transparent and its average SHG effect (~ 1 pm/V) was relatively small for an effective NLO output with high efficiency. However, from a molecular engineering point of view, urea has the potential to enlarge the bandgap and enhance the SHG effect. First, the dangling bonds of oxygen and nitrogen atoms in urea have not been totally removed so that the electronic states are not enough localized. If these nonbonding states can be eliminated as much as possible, the corresponding E_g would be enlarged into the deep-UV region. Second, the dipole moment of N–C and C–O bond is somewhat counteracted due to the close bond length and

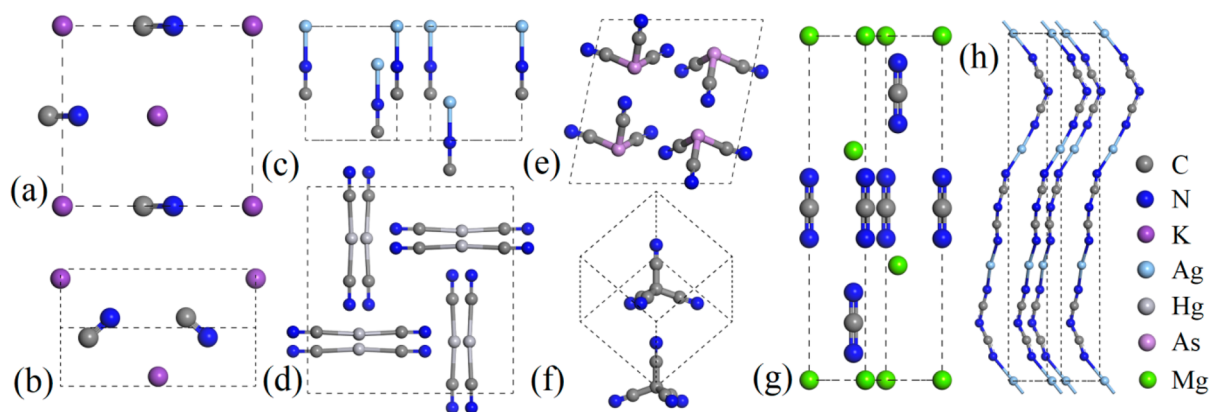


Figure 2. Structures of (a) α -KCN, (b) β -KCN, (c) AgCN, (d) HgC_2N_2 , (e) AsC_3N_3 , (f) CC_4N_4 , (g) MgCN_2 , and (h) AgC_2N_3 .

nonparallel polarized arrangement so that the micro polarity and corresponding second-order susceptibilities of $\text{CO}(\text{NH}_2)_2$ unit are not large enough. If the oxygen atoms can be substituted by other elements such as halogen or chalcogen, the dipole and NLO effect would be strengthened. In short, the systems containing the CN bond could exhibit larger SHG effect and wider bandgap. Therefore, it is interesting to evaluate the NLO performances by engineering the CN-gene into various material systems.

3.1. Linear and NLO Properties of CN-Based Materials. Cyano-based compounds are those containing the CN unit (i.e., cyano group). According to the coordination diversity around CN units as shown in Figure 1, these compounds can be mainly classified as three classes: (1) metal cyanides with relatively isolated CN units, (2) cyanogen halides with CN-based molecules, and (3) metal cyanogen chalcogenides with CN-based anionic groups. Several typical CN-based compounds (totally 16) are selected from Inorganic Crystal Structure Database (ICSD, FIZ Karlsruhe 2018, Version 3.7.0) as representatives to show the NLO properties for the first time. Their crystallographic data are listed in Table S1, with a good agreement between calculated and experimental results.

3.1.1. Structural Evolution of Metal Cyanides. Potassium cyanide (KCN) is one of the most typical metal cyanides, which has several crystal phases in the experiments. The studied phases here are two noncentrosymmetric structures as shown in Figure 2a, b,^{36,37} both of which consist of two pairs of isolated CN^- anionic units and K^+ cations. The calculated NLO capabilities including energy bandgap E_g , SHG coefficients d_{ij} , birefringence Δn (default at practical 1064 nm), UV cutoff edge λ_{UV} , and shortest SHG output wavelength λ_{PM} are listed in Table 2. It is found that both phases of KCN exhibit wide bandgap ($E_g > 7.0$ eV), large birefringence ($\Delta n > 0.1$) and available SHG effect ($1\sim 2 \times \text{KDP}$) for deep-UV NLO generation. In particular, the shortest SHG output for β -KCN is at 180 nm so that it can achieve the practical 193.7 nm coherent light output.³⁸ Though the SHG effect $d_{11} = 0.59$ pm/V is larger than that of KBBF (~ 0.5 pm/V), it is still relatively weak to achieve a sufficiently high conversion efficiency (e.g., $|d_{ij}|_{\text{max}} > 3$ pm/V). This is mainly due to the small polarity of isolated C–N bond in which the lone electron pairs on C and N atoms are in opposite orientations so the second-order polarization is canceled to some extent. Therefore, if some coordination metal elements could be introduced

Table 2. Calculated Linear and NLO Properties of KCN, AgCN, HgC_2N_2 , AsC_3N_3 , CC_4N_4 , MgCN_2 , and AgC_2N_3

	E_g (eV)	$ d_{ij} _{\text{max}}$ (pm/V) (\times urea)	Δn	λ_{UV} (nm)	λ_{PM} (nm)
α -KCN	7.11	$d_{15} = 0.76$ (0.41)	0.117	175	198
β -KCN	7.60	$d_{11} = 0.59$ (0.32)	0.121	164	180
AgCN	3.22	$d_{33} = 1.73$ (0.93)	0.238	386	386
HgC_2N_2	6.40	0	0.141	194	N/A
AsC_3N_3	5.96	$d_{22} = 0.71$ (0.40)	0.123	208	235
CC_4N_4	7.91	$d_{33} = 1.12$ (0.62)	0.001	157	N/A
MgCN_2	5.86	0	0.726	212	N/A
AgC_2N_3	4.21	0	0.560	295	N/A

to coordinate with the CN dipole unit, the polarity and corresponding NLO response would be enlarged.

AgCN satisfies such a condition as shown in Figure 2c, in which Ag^+ is connected to the end of CN unit.³⁹ It does possess much larger SHG effect and birefringence (1.73 pm/V and 0.238, see Table 2) than those of KCN due to the enlargement of covalent structural anisotropy. However, with the increase of coordination numbers from 1 to 4, the structural anisotropy is decreased from AgCN to HgC_2N_2 ,⁴⁰ AsC_3N_3 ⁴¹ and CC_4N_4 ⁴² (for structures, see Figure 2c–f), corresponding to the birefringence from 0.24 to 0.14, 0.12, and 0.00. Thus, the parallel arrangement of CN chains is most favorable for the sufficient optical anisotropy. Note that AgCN has a smaller bandgap than KCN because the hybrid orbitals of Ag and CN contribute more states in the regions around the bandgap due to the p–d coupling (for details, see Figure S2). Meanwhile, for AsC_3N_3 , the pyramidal-like molecule exhibits a large SHG effect due to the lone electron pairs on As^{3+} . However, it is not sufficiently strong (close to the α -KCN effect) because of the antiparallel polar alignment. Our further SHG density analysis as shown in Figure S2 illustrates that the SHG response is derived from the CN dipole and As^{3+} lone pairs, and the latter plays a dominate role in determining the SHG effect.¹⁶

In fact, there is another way to expand the optical anisotropy in this system, i.e., using N–C–N anions to replace the C–N anions. MgCN_2 is a typical example with N–C–N units (see Figure 2g),⁴³ exhibiting giant optical birefringence ($\Delta n \approx 0.73$), comparable to that of quasi-1D BaTiS_3 crystal (~ 0.76 in the IR region),¹ although its SHG effect vanishes due to the nonpolar N–C–N units. Similar case is AgC_2N_3 as shown in Figure 2h, in which two N–C–N chains are bridged by Ag to form 1D infinite N–C–N–Ag–N–C–N screw structures with

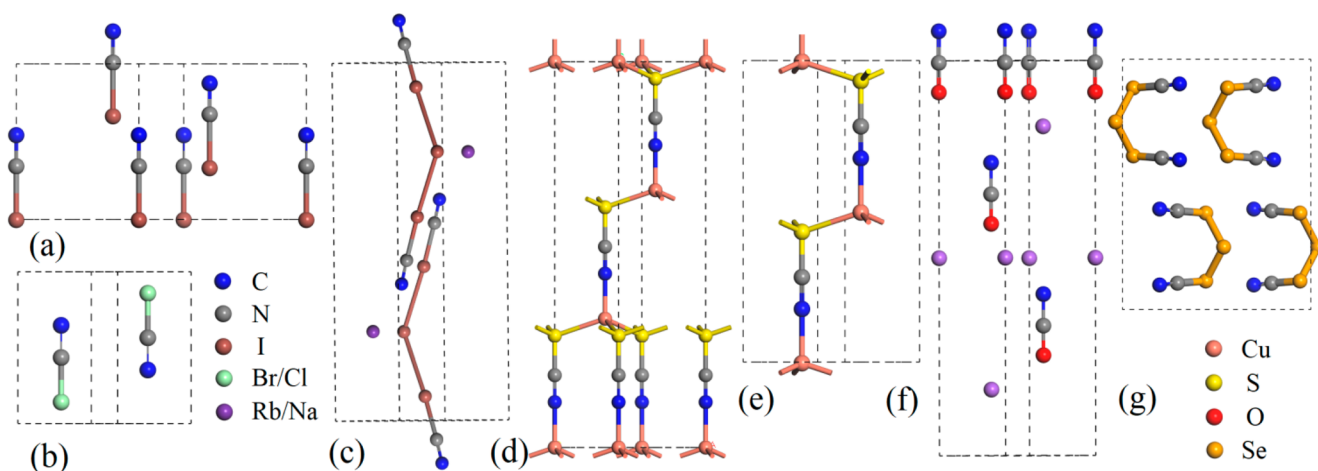


Figure 3. Structures of (a) CNI, (b) CNBr/Cl, (c) $\text{RbC}_2\text{N}_2\text{I}_3$, (d) $\alpha\text{-CuCNS}$, (e) $\beta\text{-CuCNS}$, (f) NaCNO, and (g) $\text{C}_2\text{N}_2\text{Se}_3$.

giant birefringence about 0.56.⁴⁴ It can be also imagined that the optical anisotropy could be improved by forming some anisotropic anionic groups like CNI^{2-} or CNO^{3-} , which would exhibit suitable birefringence as well as NLO capability. However, based on chemical considerations, CN^- anionic units in KCN would become CN^+ cationic units due to the difference of electronegativity between C/N and I/O, as in the cases of cyanogen halide (e.g., CNI)⁴⁵ or cyanogen chalcogenide (e.g., CuCNS)^{46,47} that will be discussed in the following sections.

3.1.2. Cyanogen Halides with Chained Molecules. Cyanogen halides are a group of chemically reactive compounds containing one cyano group (CN) attached to one halogen anion, such as fluorine, chlorine, bromine, or iodine. Among them, cyanogen iodide (CNI) (space group $R3m$), which has been synthesized in experiments,⁴⁵ is an acentric molecule structure consisting of chained CN-I molecules as displayed in Figure 3a. The C–I bond (~ 2.03 Å) is 2 times longer than the C–N bond (~ 1.19 Å) so that the spatial anisotropy along the chained direction is greatly enlarged. Therefore, the optical birefringence ($\Delta n \approx 0.74$) and SHG effect ($d_{33} \approx 17$ pm/V) listed in Table 3 are

Table 3. Calculated Linear and NLO Properties of CNI, CNBr, CNCl, $\text{RbC}_2\text{N}_2\text{I}_3$, CuCNS, NaCNO, and $\text{C}_2\text{N}_2\text{Se}_3$

	E_g (eV)	$ d_{ij} _{\text{max}}$ (pm/V) (\times urea)	Δn	λ_{UV} (nm)	λ_{PM} (nm)
CNI	5.34	$d_{33} = 16.95$ (9.1)	0.737	233	233
CNBr	6.49	0	0.741	190	N/A
CNCl	7.36	0	0.678	169	N/A
$\text{RbC}_2\text{N}_2\text{I}_3$	4.12	0	0.651	302	N/A
$\alpha\text{-CuCNS}$	2.37	$d_{33} = 8.40$ (4.5)	0.626	524	524
$\beta\text{-CuCNS}$	2.49	$d_{31} = 5.70$ (3.1)	0.590	500	500
NaCNO	5.20	$d_{33} = 0.66$ (0.4)	0.374	239	239
$\text{C}_2\text{N}_2\text{Se}_3$	3.41	0	0.329	365	N/A

significantly enhanced compared to KCN with isolated CN unit ($\Delta n \approx 0.1$ and $d_{15} \approx 0.8$ pm/V), and larger than many important NLO materials such as BBO, KTP and AGS. Although its bandgap E_g (~ 5.3 eV) is not located in the deep-UV region, it can be still transparent to most UV light from 400 to 233 nm. Moreover, the shortest phase-matching wavelength λ_{PM} is at the absorption edge of 233 nm, indicating that it can achieve the fourth harmonic generation (266 nm)

for the most practical Nd:YAG 1064 nm laser, which is greatly demanded in current laser sources.⁴⁸ From the analysis, it can be concluded that CNI is a novel NLO material with excellent NLO capabilities including large bandgap E_g , strong SHG effect d_{ij} and giant birefringence Δn . Such balanced NLO performances have never been reported up to date. The calculated band structures and partial density of states of CNI as well as urea are analyzed in Figure S3 to understand the underlying bandgap and SHG mechanism.

If the coordinated iodine is replaced by bromine, chlorine, or even fluorine, the system is possibly transparent to the deep-UV light. In fact, CNBr and CNCl have two known crystal phases.^{49,50} Their energy bandgaps are indeed enlarged to 6.5 and 7.4 eV, respectively, corresponding to the transparent edge $\lambda_{\text{UV}} \approx 190$ and 169 nm. They also exhibit extremely large birefringence ($\Delta n \approx 0.74$ and 0.68, see Table 3) close to that of CNI. Unfortunately, CNBr and CNCl are both centrosymmetric, in which the chained CNBr or CNCl polar molecules are arranged in an antiparallel manner as shown in Figure 3b, so they cannot be used in any second-order NLO process. If the total polarity can be kept in one direction as in the case of CNI, the phases of CNBr and CNCl would be possible to possess the favorable deep-UV SHG capabilities. As a test, CNBr and CNCl with $R3m$ are designed theoretically to investigate the NLO capability in the deep-UV region. It is found from Table S2 that as the halogen element changes from iodine to chlorine: (1) E_g becomes more and more larger so that CNBr and CNCl are able to transparent for a deep-UV light with the optical absorption edge $\lambda_{\text{UV}} \approx 191$ and 175 nm respectively; (2) d_{33} decreases from about 17 pm/V to 3.8 pm/V but still well satisfies the requirement for deep-UV NLO response ($> \text{KBBF}$); (3) Δn reduces from 0.7 to 0.6 although being large enough for the phase-matching condition; and (4) λ_{PM} is blue-shifted from 216 to 175 nm so CNBr and CNCl have the ability to realize the possible deep-UV SHG output.

To show if the noncentrosymmetric phases exist or not, the phonon spectra of CNBr and CNCl are further calculated by first-principles methods to confirm the dynamical stabilities,^{51,52} which are plotted in Figure S4. Note that none imaginary phonon frequency is observed in CNBr and CNCl, which demonstrates that they are both dynamically stable. In addition, the full elastic tensors c_{ij} of CNBr and CNCl are determined using the finite strain technique to confirm the Born criterion for a lattice to be stable.⁵³ From the results (for

CNBr: $c_{11} = 17.4$, $c_{33} = 127.0$, $c_{44} = 3.4$, $c_{12} = 6.9$, $c_{13} = 2.2$, $c_{14} = -2.3$; for CNCl: $c_{11} = 19.4$, $c_{33} = 110.7$, $c_{44} = 3.4$, $c_{12} = 7.8$, $c_{13} = 3.0$, $c_{14} = -2.4$; unit is GPa), it is easy to verify the general conditions for stability, $(c_{11} + c_{12}) \times c_{33} - 2 \times c_{13}^2 > 0$ and $(c_{11} - c_{12}) \times c_{44} - 2 \times c_{14}^2 > 0$ are satisfied.

It should be also noted that there is one cyanogen halide compound, i.e., $\text{RbC}_2\text{N}_2\text{I}_3$, in which two CNI molecules are bridged by iodine to form one CNI-I-CNI chain like “nunchakus” as shown in Figure 3c.⁵⁴ Its birefringence is smaller than those of CNX (X = Cl, Br, I) because of the nonparallel arrangement of CNI chains but it is still giant ($\Delta n \approx 0.65$). Similar structural and optical features can also be found in $\text{KC}_2\text{N}_2\text{I}$.⁵⁵

3.1.3. Cyanogen Chalcogenides with Chained CN-Based Anionic Groups. Cyanogen chalcogenides usually consist of an isolated metal cation and a cyano group (CN) attached to the chalcogen anion. Figure 3d, e show two known phases of copper cyanogen sulfide CuCNS , with space group of $P6_3mc$ and $R3m$, respectively.^{46,47} In both structures, CNS^- dipole units are arranged in a polarity-parallel manner along the c -axis, which is beneficial to enhance the SHG effect and birefringence. As listed in Table 3, they indeed exhibit sufficiently large $|d_{ij}|_{\text{max}}$ (~ 5.7 and 8.4 pm/V) and giant Δn (~ 0.59 and 0.63), although their bandgaps are lower than 3 eV. The analogue NaCN O exhibits large birefringence ($\Delta n \approx 0.35$) as well, but its SHG effect becomes relatively smaller due to the close bond length of C–N and C–O but opposite direction (see Figure 3f).⁵⁶ If the oxygen is replaced by sulfur, selenium or tellurium, the corresponding SHG effect would be enhanced accordingly. This can be also concluded from the calculated NLO capabilities of theoretically designed NaCNX (X = S, Se, Te) in Table S2. Note that all of them can achieve the available IR conversion efficiency with the SHG effect from 10 to $53 \times \text{KDP}$ and keep sufficiently large birefringence (> 0.3) for the phase-matching conditions. However, all of these cyanogen chalcogenides exhibit relatively smaller bandgap than that of CNI ($E_g \approx 5.3$ eV) so they cannot be applied in the deep-UV region.

In fact, some other CN-based compounds with novel chain structures, e.g., $\text{C}_2\text{N}_2\text{Se}_3$, $\text{C}_2\text{N}_2\text{S}_2$, $\text{PbC}_2\text{N}_2\text{S}_2$, $\text{CdHgC}_4\text{N}_4\text{S}_4$, $\text{HgC}_2\text{N}_2\text{Se}_2$, CNSCl , PbCNSCl , SnCNSF , etc.,^{57–64} can also exhibit very large structural anisotropy. For example, $\text{C}_2\text{N}_2\text{Se}_3$ has a novel “U-type” unit where one Se atom is linked with two CNSe chains (see Figure 3g),⁵⁷ thus exhibiting a large optical birefringence about 0.33 (see Table 3).

3.2. Prospect for the CN-Based Compounds as NLO and/or Birefringent Materials. To evaluate the prospect of CN-based compounds for the optical applications, in Figure 4 we summarize the energy bandgap E_g , SHG effect d_{ij} and birefringence Δn of the studied metal cyanides, cyanogen halides and cyanogen chalcogenides as well as many typical NLO materials across from IR to UV regions.^{65–76} In Figure 4a, the red squares represent the IR NLO materials such as AGS ,⁹ AgGaSe_2 ,⁶⁵ Ag_3AsS_3 ,⁶⁶ BaGa_4S_7 ,⁶⁷ BaGa_4Se_7 ,⁶⁸ ZnGeP_2 ,⁶⁹ CsGeCl_3 ,⁷⁰ LiIO_3 ,⁷ LN ,⁸ etc. and the purple circles are the UV materials with NLO effect such as KBBF ,⁴ BBO ,⁵ LBO ,⁶ BiB_3O_6 ,⁷¹ etc. (for details, see Table S3); the green (or blue) shaded region represents the preferred area for IR (or UV) generation with high conversion efficiency. For CN-based compounds marked by black pentagrams, it can be concluded that (1) the SHG effect is across a wide range from about 1 to 54 times of KDP, and the bandgap spans from 7.9 to 2.3 eV; and (2) seven compounds exhibit larger SHG effect than $10 \times$

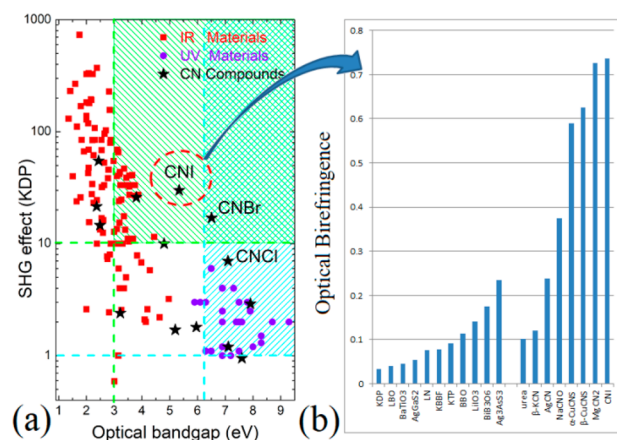


Figure 4. (a) Energy bandgap and SHG effect, and (b) optical birefringence of CN-based compounds as well as many typical IR and UV NLO materials.

KDP, and five have larger bandgap than the deep-UV edge. Both demonstrate that the CN-based compounds can exhibit tunable NLO capabilities with wide transparency. Remarkably, CNI is a promising NLO material candidate expected to be applied in the regions from IR to UV due to the balanced NLO performances, which has not been achieved practically up to date. Moreover, for the materials with bandgap > 5 eV, CNI possesses so far the largest SHG effect ($\sim 30 \times \text{KDP}$), about 10 times larger than that of BBO ($\sim 3 \times \text{KDP}$).

Furthermore, the optical birefringences of CN-based compounds are compared with those of practical NLO crystals as shown in Figure 4b. It is found that basically the birefringences of typical NLO materials are below 0.3 (e.g., $\Delta n \approx 0.23$ for Ag_3AsS_3).⁶⁶ For CN-based compounds, most of them have larger birefringence than 0.1, and some exhibit giant birefringence larger than 0.5 (e.g., $\Delta n \approx 0.7$ for CNI and MgCN_2). The unprecedented degree of optical anisotropy will be broadly useful for next-generation imaging, communications and sensing applications, in particular for miniaturized photonic devices with wide transparent range, which is also expected for them to possess sufficiently large electrical, thermal, and other physical anisotropies.¹

In this sense, the CN unit is a heretofore unrecognized but unique NLO and birefringent material gene, which can make materials to achieve the tunable NLO capability not only for the IR and UV SHG output but also for the optical birefringent modulation.^{77,78} Once confirmed in the experiment, it would greatly promote the development of optical devices and lasers operating in the wide regions spanning from IR to UV spectra. Of course, in inorganic cyanides, the salts (e.g., potassium cyanide) are highly toxic. Cyanogen iodide is also a relatively volatile and highly toxic inorganic compound. It occurs as white crystals that react slowly with water to form hydrogen cyanide, which is a highly volatile liquid that is produced on a large scale industrially. In practice, there are some applications for cyanides, which are mainly produced for the mining of gold and silver, and are also used in electroplating, jewelry-making, and certain kinds of photography such as sepia toning.⁷⁹ In applications, they can be synthesized and stored in a relatively safe way although better safety and green synthesis strategies are still needed.

4. CONCLUSION

Over the last decades, some basic structural motifs such as $(\text{BO}_3)^{3-}$, $(\text{B}_3\text{O}_6)^{3-}$, $(\text{B}_3\text{O}_7)^{5-}$, $(\text{H}_2\text{PO}_4)^-$, $(\text{TiO}_6)^{8-}$, $(\text{NbO}_6)^{7-}$, and $(\text{GaS}_4)^{5-}$, are considered as good NLO material genome that can realize the coherent light with high output power from UV to IR regions (0.2–2 μm), but none of them are performing-balanced NLO units with wide transparency, strong NLO effect and large birefringence across from IR to deep-UV regions due to the relative small optical anisotropy. Importantly in our study, the chained CN motif is discovered to exhibit the promising NLO capability both in IR and deep-UV regions by investigating the linear and NLO properties of several series of CN-based systems, including metal cyanides, cyanogen halides and cyanogen chalcogenides. Interestingly, we can tune the structural polarity and coordination environment by attaching appropriate elements to the NLO-active CN units to improve the NLO or birefringent performances. As representatives, (1) the known β -KCN can achieve the deep-UV SHG output of 193.7 nm with high conversion efficiency; (2) the chained acentric CNI structure, which has been obtained in the experiment, can achieve the frequency conversion at UV 266 nm with sufficiently large NLO effect and giant optical birefringence; (3) the theoretically stable analogues CNBr and CNCl can achieve the practical 177.3 nm output in the deep-UV region with giant birefringence as well. Upon being confirmed by experiments, the CN-based materials would greatly promote the understanding of NLO material genome and provide promising candidates with giant optical anisotropy for potential IR and UV optical applications.

■ ASSOCIATED CONTENT

Supporting Information

The Supporting Information is available free of charge on the ACS Publications website at DOI: 10.1021/acs.inorgchem.8b02795.

Tables S1–S3 and Figures S1–S4, including unit-cell structure of urea crystal; experimental and calculated unit-cell parameters of the studied CN-based compounds; partial density of states of KCN and AgCN; SHG density of AsC_3N_3 ; band structures and partial density of states of urea and CNI; calculated NLO capabilities of CNX ($X = \text{I, Br, Cl}$) and NaCNX ($X = \text{S, Se, Te}$); calculated phonon spectra of CNX ($X = \text{I, Br, Cl}$); and the bandgap E_g and SHG effect d_{ij} of typical IR and UV NLO crystals (PDF)

■ AUTHOR INFORMATION

Corresponding Authors

*E-mail: zslin@mail.ipc.ac.cn (Z.L.).

*E-mail: bing.huang@csr.ac.cn (B.H.).

ORCID

Lei Kang: 0000-0002-9993-6399

Fei Liang: 0000-0002-4932-1329

Zheshuai Lin: 0000-0002-9829-9893

Feng Liu: 0000-0002-3701-8058

Notes

The authors declare no competing financial interest.

■ ACKNOWLEDGMENTS

This work was supported by NSFC Grants 11574024, 91622118, 11704023, and NSAF U1530401. F.L. acknowledges support from US DOE-BES (DE-FG02-04ER46148). Z.L. acknowledges support from the Outstanding Member in Youth Innovation Promotion Association at CAS.

■ REFERENCES

- (1) Niu, S.; Joe, G.; Zhao, H.; Zhou, Y.; Orvis, T.; Huyan, H.; Salman, J.; Mahalingam, K.; Urwin, B.; Wu, J.; Liu, Y.; Tiwald, T.; Cronin, S.; Howe, B.; Mecklenburg, M.; Haiges, R.; Singh, D.; Wang, H.; Kats, M.; Ravichandran, J. Giant Optical Anisotropy in A Quasi-One-Dimensional Crystal. *Nat. Photonics* **2018**, *12*, 392.
- (2) Becker, P. Borate Materials in Nonlinear Optics. *Adv. Mater.* **1998**, *10*, 979–992.
- (3) Chung, I.; Kanatzidis, M. Metal Chalcogenides: A Rich Source of Nonlinear Optical Materials. *Chem. Mater.* **2014**, *26*, 849–869.
- (4) Chen, C. T.; Wang, G. L.; Wang, X.; Xu, Z. Deep-UV Nonlinear Optical Crystal $\text{KBe}_2\text{BO}_3\text{F}_2$ -Discovery, Growth, Optical Properties and Applications. *Appl. Phys. B: Lasers Opt.* **2009**, *97*, 9–25.
- (5) Chen, C. T.; Wu, B.; Jiang, A.; You, G. A New-Type Ultraviolet SHG Crystal - Beta- BaB_2O_4 . *Sci. Sin. Ser. B* **1985**, *28*, 235–243.
- (6) Chen, C. T.; Wu, Y. C.; Jiang, A. D.; Wu, B. C.; You, G. M.; Li, R. K.; Lin, S. J. New Nonlinear-Optical Crystal - LiB_3O_5 . *J. Opt. Soc. Am. B* **1989**, *6*, 616–621.
- (7) Eckardt, R.; Masuda, H.; Fan, Y.; Byer, R. Absolute and Relative Nonlinear Optical Coefficients of KDP, BaB_2O_4 , LiIO_3 , MgO-LiNbO_3 and KTP Measured by Phase-Matched 2nd-Harmonic Generation. *IEEE J. Quantum Electron.* **1990**, *26*, 922–933.
- (8) Boyd, G. D.; Nassau, K.; Miller, R. C.; Bond, W. L.; Savage, A. LiNbO_3 - Efficient Phase Matchable Nonlinear Optical Material (Uniaxial Piezoelectric Optical Parametric Effects E). *Appl. Phys. Lett.* **1964**, *5*, 234–236.
- (9) Okorogu, A. O.; Mirov, S. B.; Lee, W.; Crouthamel, D. I.; Jenkins, N.; Dergachev, A. Y.; Vodopyanov, K. L.; Badikov, V. V. Tunable Middle Infrared Downconversion in GaSe and AgGaS_2 . *Opt. Commun.* **1998**, *155*, 307–312.
- (10) Chen, C. T.; Ye, N.; Lin, J.; Jiang, J.; Zeng, W. R.; Wu, B. C. Computer-Assisted Search for Nonlinear Optical Crystals. *Adv. Mater.* **1999**, *11*, 1071–1077.
- (11) Boyd, R. *Nonlinear Optics*, 3rd ed.; Academic Press, 2008; pp 79–84.
- (12) Chen, C.; Lin, Z.; Wang, Z. The Development of New Borate-Based UV Nonlinear Optical Crystals. *Appl. Phys. B: Lasers Opt.* **2005**, *80*, 1–25.
- (13) Tran, T. T.; Yu, H. W.; Rondinelli, J. M.; Poeppelmeier, K. R.; Halasyamani, P. S. Deep Ultraviolet Nonlinear Optical Materials. *Chem. Mater.* **2016**, *28*, 5238–5258.
- (14) Kang, L.; Ramo, D.; Lin, Z. S.; Bristowe, P. D.; Qin, J. G.; Chen, C. T. First Principles Selection and Design of Mid-IR Nonlinear Optical Halide Crystals. *J. Mater. Chem. C* **2013**, *1*, 7363–7370.
- (15) Kang, L.; Zhou, M. L.; Yao, J. Y.; Lin, Z. S.; Wu, Y. C.; Chen, C. T. Metal Thiophosphates with Good Mid-infrared Nonlinear Optical Performances: A First-Principles Prediction and Analysis. *J. Am. Chem. Soc.* **2015**, *137*, 13049–13059.
- (16) Lin, Z. S.; Jiang, X. X.; Kang, L.; Gong, P. F.; Luo, S. Y.; Lee, M. H. First-Principles Materials Applications and Design of Nonlinear Optical Crystals. *J. Phys. D: Appl. Phys.* **2014**, *47*, 253001.
- (17) Payne, M. C.; Teter, M. P.; Allan, D. C.; Arias, T. A.; Joannopoulos, J. D. Iterative Minimization Techniques for Abinitio Total-Energy Calculations - Molecular-Dynamics And Conjugate Gradients. *Rev. Mod. Phys.* **1992**, *64*, 1045–1097.
- (18) Clark, S. J.; Segall, M. D.; Pickard, C. J.; Hasnip, P. J.; Probert, M. J.; Refson, K.; Payne, M. C. First Principles Methods Using CASTEP. *Z. Kristallogr. - Cryst. Mater.* **2005**, *220*, 567–570.

- (19) Rappe, A. M.; Rabe, K. M.; Kaxiras, E.; Joannopoulos, J. D. Optimized Pseudopotentials. *Phys. Rev. B: Condens. Matter Mater. Phys.* **1990**, *41*, 1227–1230.
- (20) Monkhorst, H. J.; Pack, J. D. Special Points for Brillouin-Zone Integrations. *Phys. Rev. B* **1976**, *13*, 5188–5192.
- (21) Pfrommer, B. G.; Cote, M.; Louie, S. G.; Cohen, M. L. Relaxation of Crystals with the Quasi-Newton method. *J. Comput. Phys.* **1997**, *131*, 233–240.
- (22) Asahi, R.; Mannstadt, W.; Freeman, A. J. Optical Properties and Electronic Structures of Semiconductors with Screened-Exchange LDA. *Phys. Rev. B: Condens. Matter Mater. Phys.* **1999**, *59*, 7486–7492.
- (23) Ceperley, D. M.; Alder, B. J. Ground-State of the Electron-Gas by A Stochastic Method. *Phys. Rev. Lett.* **1980**, *45*, 566–569.
- (24) Lin, J.; Lee, M. H.; Liu, Z. P.; Chen, C. T.; Pickard, C. J. Mechanism for Linear and Nonlinear Optical Effects in Beta-BaB₂O₄ Crystals. *Phys. Rev. B: Condens. Matter Mater. Phys.* **1999**, *60*, 13380–13389.
- (25) Lin, Z. S.; Wang, Z. H.; Chen, C. T.; Lee, M. H. Mechanism of Linear and Nonlinear Optical Effects of KDP and Urea Crystals. *J. Chem. Phys.* **2003**, *118*, 2349–2356.
- (26) Halasyamani, P.; Rondinelli, J. The Must-Have and Nice-to-Have Experimental and Computational Requirements for Functional Frequency Doubling Deep-UV Crystals. *Nat. Commun.* **2018**, *9*, 2972.
- (27) He, R.; Huang, H.; Kang, L.; Yao, W.; Jiang, X.; Lin, Z.; Qin, J.; Chen, C. Bandgaps in the Deep Ultraviolet Borate Crystals: Prediction and Improvement. *Appl. Phys. Lett.* **2013**, *102*, 231904.
- (28) Liang, F.; Kang, L.; Lin, Z. S.; Wu, Y. C. Mid-Infrared Nonlinear Optical Materials Based on Metal Chalcogenides: Structure-Property Relationship. *Cryst. Growth Des.* **2017**, *17*, 2254–2289.
- (29) Kang, L.; Luo, S. Y.; Peng, G.; Ye, N.; Wu, Y. C.; Chen, C. T.; Lin, Z. S. First-Principles Design of a Deep-Ultraviolet Nonlinear-Optical Crystal from KBe₂BO₃F₂ to NH₄Be₂BO₃F₂. *Inorg. Chem.* **2015**, *54*, 10533–10535.
- (30) Zhou, M. L.; Kang, L.; Yao, J. Y.; Lin, Z. S.; Wu, Y. C.; Chen, C. T. Midinfrared Nonlinear Optical Thiophosphates from LiZnPS₄ to AgZnPS₄: A Combined Experimental and Theoretical Study. *Inorg. Chem.* **2016**, *55*, 3724–3726.
- (31) Liang, F.; Kang, L.; Gong, P. F.; Lin, Z. S.; Wu, Y. C. Rational Design of Deep-Ultraviolet Nonlinear Optical Materials in Fluorooxoborates: Toward Optimal Planar Configuration. *Chem. Mater.* **2017**, *29*, 7098–7102.
- (32) Liang, F.; Kang, L.; Lin, Z. S.; Wu, Y. C.; Chen, C. T. Analysis and Prediction of Mid-IR Nonlinear Optical Metal Sulfides with Diamond-Like Structures. *Coord. Chem. Rev.* **2017**, *333*, 57–70.
- (33) Peng, G.; Ye, N.; Lin, Z. S.; Kang, L.; Pan, S.; Zhang, M.; Lin, C.; Long, X.; Luo, M.; Chen, Y.; Tang, Y.; Xu, F.; Yan, T. NH₄Be₂BO₃F₂ and γ -Be₂BO₃F: Overcoming the Layering Habit in KBe₂BO₃F₂ for the Next Generation Deep-Ultraviolet Nonlinear Optical Materials. *Angew. Chem., Int. Ed.* **2018**, *57*, 8968–8972.
- (34) Kang, L.; Lin, Z. S.; Liu, F.; Huang, B. Removal of A-Site Alkali and Alkaline Earth Metal Cations in KBe₂BO₃F₂-Type Layered Structures To Enhance the Deep-Ultraviolet Nonlinear Optical Capability. *Inorg. Chem.* **2018**, *57*, 11146–11156.
- (35) Liu, T.; Qin, J.; Zhang, G.; Zhu, T.; Niu, F.; Wu, Y.; Chen, C. Mercury Bromide (HgBr₂): A Promising Nonlinear Optical Material in IR Region with A High Laser Damage Threshold. *Appl. Phys. Lett.* **2008**, *93*, 091102.
- (36) Decker, D. L.; Beyerlein, R. A.; Roullet, G.; Worlton, T. G. Neutron-Diffraction Study of KCN III and KCN IV at High Pressure. *Phys. Rev. B* **1974**, *10*, 3584–3593.
- (37) Rowe, J. M.; Rush, J. J.; Susman, S. Neutron Powder Diffraction Study of Phase-Transitions and Structures of (KCN)_x(KBr)_{1-x} Mixed-Crystals. *Phys. Rev. B: Condens. Matter Mater. Phys.* **1983**, *28*, 3506–3511.
- (38) Chen, C. T.; Luo, S. Y.; Wang, X. Y.; Wang, G. L.; Wen, X. H.; Wu, H. X.; Zhang, X.; Xu, Z. Y. Deep UV Nonlinear Optical Crystal: RbBe₂(BO₃)F₂. *J. Opt. Soc. Am. B* **2009**, *26*, 1519–1525.
- (39) Bowmaker, G.; Kennedy, B.; Reid, J. Crystal Structures of AuCN and AgCN and Vibrational Spectroscopic Studies of AuCN, AgCN, and CuCN. *Inorg. Chem.* **1998**, *37*, 3968–3974.
- (40) Zhdanov, G. S.; Sugam, E. A. The Crystal Structure of Mercuric Cyanide. *Dokl. Akad. Nauk SSSR* **1944**, *45*, 312–314.
- (41) Emerson, K.; Britton, D. The Crystal and Molecular Structure of Arsenic Tricyanide. *Acta Crystallogr.* **1963**, *16*, 113–118.
- (42) Britton, D. The Crystal Structure of Tetracyanomethane, C(CN)₄. *Acta Crystallogr., Sect. B: Struct. Crystallogr. Cryst. Chem.* **1974**, *30*, 1818–1821.
- (43) Berger, U.; Schnick, W. Syntheses, Crystal Structures and Vibrational Spectroscopic Properties of MgCN₂, SrCN₂ and BaCN₂. *J. Alloys Compd.* **1994**, *206*, 179–184.
- (44) Britton, D.; Chow, Y. M. Crystal Structure of Silver Dicyanamide, AgN(CN)₂. *Acta Crystallogr., Sect. B: Struct. Crystallogr. Cryst. Chem.* **1977**, *33*, 697–699.
- (45) Ketelaar, J.; Zwartsenberg, J. The Crystal Structure of the Cyanogen Halides. I. The Structure of Cyanogen Iodide. *Recueil Des Travaux Chimiques Des Pays-Bas* **1939**, *58*, 448–452.
- (46) Smith, D. L.; Saunders, V. I. The Structure and Polytypism of the Beta-Modification of Copper(I) Thiocyanate. *Acta Crystallogr., Sect. B: Struct. Crystallogr. Cryst. Chem.* **1981**, *37*, 1807–1812.
- (47) Smith, D. L.; Saunders, V. I. Preparation and Structure Refinement of the 2h-Polytype of Beta-Copper(I) Thiocyanate. *Acta Crystallogr., Sect. B: Struct. Crystallogr. Cryst. Chem.* **1982**, *38*, 907–909.
- (48) Wang, G.; Geng, A.; Bo, Y.; Li, H.; Sun, Z.; Bi, Y.; Cui, D.; Xu, Z.; Yuan, X.; Wang, X.; Shen, G.; Shen, D. 284 W 266 nm Ultraviolet-Beam Generation by Fourth-Harmonic Generation of an All-Solid-State Laser. *Opt. Commun.* **2006**, *259*, 820–822.
- (49) Geller, S.; Schawlow, A. Crystal Structure and Quadrupole Coupling of Cyanogen Bromide BrCN. *J. Chem. Phys.* **1955**, *23*, 779–783.
- (50) Heiart, R. B.; Carpenter, G. B. The Crystal Structure of Cyanogen Chloride. *Acta Crystallogr.* **1956**, *9*, 889–895.
- (51) Baroni, S.; de Gironcoli, S.; Dal Corso, A.; Giannozzi, P. Phonons and Related Crystal Properties from Density-Functional Perturbation Theory. *Rev. Mod. Phys.* **2001**, *73*, 515–562.
- (52) Yao, Y.; Tse, J.; Sun, J.; Klug, D.; Martonak, R.; Iitaka, T. Comment on "New Metallic Carbon Crystal". *Phys. Rev. Lett.* **2009**, *102*, 9601.
- (53) Karki, B. B.; Ackland, G. J.; Crain, J. Elastic Instabilities in Crystals from Ab Initio Stress-Strain Relations. *J. Phys.: Condens. Matter* **1997**, *9*, 8579–8589.
- (54) Tebbe, K. F.; Froehlich, R. Studies on the Polypseudohalides, II Preparation and Crystal Structure of Rb[I(ICN)₂]. *Z. Naturforsch., B: J. Chem. Sci.* **1983**, 549–553.
- (55) Tebbe, K.; Krauss, N. Studies on the Polypseudohalides, II Preparation and Crystal Structure of K[I(ICN)₂]. *Z. Naturforsch., B: J. Chem. Sci.* **1988**, *43*, 149–152.
- (56) Bassiere, M. The Structure of Sodium Isocyanate. *C. R. Hebd. Seances Acad. Sci.* **1938**, *206*, 1309–1311.
- (57) Hazell, A. C. The Crystal Structures of Selenium Dicyanide and Sulphur Dicyanide. *Acta Crystallogr.* **1963**, *16*, 843–844.
- (58) Burchell, C.; Kilian, P.; Slawin, A.; Woollins, J.; Tersago, K.; van Alsenoy, C.; Blockhuys, F. E₂(CN)₂ (E = S, Se) and Related Compounds. *Inorg. Chem.* **2006**, *45*, 710–716.
- (59) Mokuolu, J. A. A.; Speakman, J. C. The Crystal Structure of Lead(II) Thiocyanate. *Acta Crystallogr., Sect. B: Struct. Crystallogr. Cryst. Chem.* **1975**, *31*, 172–176.
- (60) Fedorov, P.; Andreyanova, L.; Pachomov, V. Crystal Structure of Cadmium Mercury(ii) Thiocyanate. *Coord. Chem.* **1975**, *1*, 252–254.
- (61) Bowmaker, G. A.; Churakov, A. V.; Harris, R. K.; Howard, J. A. K.; Apperley, D. C. Solid-state (199)Hg MAS NMR Studies of Mercury(II) Thiocyanate and Related Compounds. Crystal Structure of Hg(SeCN)₂. *Inorg. Chem.* **1998**, *37*, 1734–1743.

(62) Hazell, A. C. The Crystal Structure of 2,3,7,8-Tetrachloro-5,10,11,12-Tetrathia-1,4,6,9-Tetraaza Ricyclo(5.3.1.1.)dodeca-3,8-Diene, (SNCCl)₄. *Acta Chem. Scand.* **1967**, *21*, 415–423.

(63) Gacemi, A.; Benbental, D.; Gautier Luneau, I.; Mosset, A. Crystal Structure of Lead Chloride Thiocyanate, PbCl(SCN). *Z. Kristallogr. - New Cryst. Struct.* **2005**, *220*, 309–310.

(64) Vilminot, S.; Granier, W.; Al Oraibi, Z. A.; le Cot, L. Structural Study of Tin (II) Fluoroisothiocyanate. *Acta Crystallogr., Sect. B: Struct. Crystallogr. Cryst. Chem.* **1978**, *34*, 3306–3307.

(65) Boyd, G. D.; Storz, F. G.; McFee, J. H.; Kasper, H. M. Linear and Nonlinear Optical Properties of Some Ternary Selenides. *IEEE J. Quantum Electron.* **1972**, *8*, 900–908.

(66) Feichtner, J.; Roland, G. Optical Properties of a New Nonlinear Optical Material: Tl₃AsSe₃. *Appl. Opt.* **1972**, *11*, 993–998.

(67) Lin, X.; Zhang, G.; Ye, N. Growth and Characterization of BaGa₄S₇: A New Crystal for Mid-IR Nonlinear Optics. *Cryst. Growth Des.* **2009**, *9*, 1186–1189.

(68) Yao, J. Y.; Mei, D. J.; Bai, L.; Lin, Z. S.; Yin, W. L.; Fu, P. Z.; Wu, Y. C. BaGa₄Se₇: A New Congruent-Melting IR Nonlinear Optical Material. *Inorg. Chem.* **2010**, *49*, 9212–9216.

(69) Boyd, G. D.; Buehler, E.; Storz, F. Linear and Nonlinear Optical Properties of ZnGeP₂ and CdSe. *Appl. Phys. Lett.* **1971**, *18*, 301–304.

(70) Zhang, J.; Su, N.; Yang, C.; Qin, J. G.; Ye, N.; Wu, B. C.; Chen, C. T. A New NLO Material in IR Region: CsGeCl₃. In *Electro-Optic and Second Harmonic Generation Materials, Devices, and Applications II*; Chen, C. T., Ed.; SPIE: 1998; Vol. 3556, pp 1–3.

(71) Hellwig, H.; Liebertz, J.; Bohaty, L. Exceptional Large Nonlinear Optical Coefficients in the Monoclinic Bismuth Borate BiB₃O₆ (BIBO). *Solid State Commun.* **1998**, *109*, 249–251.

(72) Lan, H.; Liang, F.; Jiang, X.; Zhang, C.; Yu, H.; Lin, Z.; Zhang, H.; Wang, J.; Wu, Y. Pushing Nonlinear Optical Oxides into the Mid-Infrared Spectral Region Beyond 10 μm: Design Synthesis, and Characterization of La₃SnGa₅O₁₄. *J. Am. Chem. Soc.* **2018**, *140*, 4684–4690.

(73) Mei, D.; Zhang, S.; Liang, F.; Zhao, S.; Jiang, J.; Zhong, J.; Lin, Z.; Wu, Y. LiGaGe₂S₆: A Chalcogenide with Good Infrared Nonlinear Optical Performance and Low Melting Point. *Inorg. Chem.* **2017**, *56*, 13267–13273.

(74) Luo, M.; Liang, F.; Song, Y.; Zhao, D.; Ye, N.; Lin, Z. Rational Design of the First Lead/Tin Fluorooxoborates MB₂O₃F₂ (M = Pb, Sn) Containing Flexible Two-Dimensional B₆O₁₂F₆ Single Layers with Widely Divergent Second Harmonic Generation Effects. *J. Am. Chem. Soc.* **2018**, *140*, 6814–6817.

(75) Luo, M.; Liang, F.; Song, Y.; Zhao, D.; Xu, F.; Ye, N.; Lin, Z. M₂B₁₀O₁₄F₆ (M = Ca, Sr): Two Noncentrosymmetric Alkaline Earth Fluorooxoborates as Promising Next-Generation Deep-Ultraviolet Nonlinear Optical Materials. *J. Am. Chem. Soc.* **2018**, *140*, 3884–3887.

(76) Song, Y.; Luo, M.; Liang, F.; Ye, N.; Lin, Z. The Second-Harmonic Generation Intensification derived from Localization Conjugated π-orbitals in O₂²⁻. *Chem. Commun.* **2018**, *54*, 1445–1448.

(77) Zhang, B.; Han, G.; Wang, Y.; Chen, X.; Yang, Z.; Pan, S. Expanding Frontiers of Ultraviolet Nonlinear Optical Materials with Fluorophosphates. *Chem. Mater.* **2018**, *30*, 5397–5403.

(78) Lei, B.; Yang, Z.; Yu, H.; Cao, C.; Li, Z.; Hu, C.; Poepplmeier, K.; Pan, S. Module-Guided Design Scheme for Deep-Ultraviolet Nonlinear Optical Materials. *J. Am. Chem. Soc.* **2018**, *140*, 10726–10733.

(79) Gail, E.; Gos, S.; Kulzer, R.; Lorosch, J.; Rubo, A.; Sauer, M.; Kellens, R.; Reddy, J.; Steier, N.; Hasenpusch, W. Cyano Compounds, Inorganic. In *Ullmann's Encyclopedia of Industrial Chemistry*; Wiley-VCH: 2011.